Direct Synthesis and Design of Wideband Bandpass Filter With Composite Series and Shunt Resonators

Zhiliang Li and Ke-Li Wu, *Fellow, IEEE*

***Abstract*— In this paper, a wideband bandpass filter with composite series and shunt resonators is proposed together with a direct synthesis and design theory. The filter configuration can provide transmission zeros (TZs) on both sides of the passband. Two types of composite shunt resonators are introduced; one provides extra controllable TZs in the far stopband, whereas the other not only produces close-to-band TZs, but also high-order TZs in the far stopband in planar realization. The composite series resonator is realized by a high-impedance transmission line in shunt with a lumped capacitor. By introducing legitimate wideband circuit model approximations for the basic circuit blocks, a mixed lumped/distributed element version of the proposed filter is realized and experimentally verified. Design flexibility of circuit topology and spurious resonance suppression using TZs is discussed. Two design examples of the fifth-order and ninth-order filter prototypes are synthesized, designed, and measured, demonstrating the effectiveness of the synthesis and design theory as well as the superior performance of the proposed filter configuration.**

***Index Terms*— Bandpass filter, composite resonators, microstrip, mixed lumped/distributed (MLD) element circuit, synthesis, transmission zeros (TZs), wideband filter.**

I. Introduction

NOWADAYS, there is an inevitable trend in integrating multiple functional radio components working in different frequency bands into one system module such as active antenna systems for base stations. To accommodate multiple frequency bands cost-effectively while providing sufficient rejection between them, multiple high-order bandpass filters are bundled into one integrated passive component that is then affixed by a wideband bandpass filter with a steep skirt selectivity and a wide and deep rejection stopband to suppress out-of-band interference and noise, which may occur in both lower and higher frequency bands.

As an intensively studied topic, various wideband bandpass filters have been proposed in the literature. Some of them use the optimum distributed high-pass filter structure [1], the cascaded low-pass/high-pass filters [2], [3], multiple-mode resonators [4], and ring resonators [5]–[7]. To enhance skirt selectivity and extend the stopband with deep rejection, transmission zeros (TZs) are commonly introduced. The existing approaches to introduce TZs for a wideband filter can be categorized as: 1) exploiting I/O cross couplings [8]; 2) using two transmission paths to achieve signal cancellation [9]–[11]; and 3) introducing short circuits at designated TZ frequencies to the main signal line of a filter [12]–[15]. Although many of these reported methods are effective for certain applications, only a few of them are equipped by a systematic synthesis and design theory that allows an optimal and deterministic design of a wideband filter with a widest stopband possible.

In the literature, there are many techniques proposed to extend the stopband of a bandpass filter. One of them is to shift spurious resonances to higher frequencies using stepped impedance resonators (SIRs) [16]. Another technique is to use dissimilar resonators having the same fundamental resonant frequency but different spurious resonances [17], [18]. Two popular ways to control spurious resonances of different resonators are: 1) by varying the characteristic impedances or lengths of high- and low-impedance sections of SIRs [17] and 2) adding stubs to the main resonators [18]. Other techniques include using periodic nonuniform coupled microstrip lines [19], coupling control at unwanted resonant frequency [20], and so on. When passband bandwidth increases, suppression of spurious resonances will be challenging as couplings among spurious resonances are strong. In [11], [12], and [15], multiple TZs can be tactically designated to achieve a wide upper stopband. The uniform connecting lines are replaced with SIRs to suppress the harmonic passbands of the filter in [21]. In [22], a combination of techniques for harmonic suppression is used to design a wideband filter, but the design heavily relies on the iterative EM simulations. Note that there are no TZs in the lower stopband in [11] and [15], which may limit their applications if a symmetrical bandpass response or a steep skirt selectivity at lower band edge is required. Though TZs are presented on both sides of the passband in [12], they are not independently controllable and the stopband rejection is only around 15 dB.

In this paper, a wideband bandpass filter that is composed of composite series and shunt resonators, as depicted in Fig. 1, is proposed. The unique feature of this filter that is distinct from that in [15] is the incorporation of composite series resonators for producing TZs below the passband, providing a full flexibility in arranging TZs on both upper and lower stopbands.

With the above-mentioned feature, the proposed wideband filter is able to provide a steep skirt selectivity at two band edges. In addition, an iterative procedure of adjusting TZs for spurious suppression is proposed, contributing to a

Manuscript received August 23, 2016; revised December 23, 2016 and March 13, 2017; accepted March 18, 2017. Date of publication April 4, 2017; date of current version October 4, 2017. This work was supported in part by the Postgraduate Scholarship of The Chinese University of Hong Kong and in part by the Development and Reform Commission of Shenzhen Municipality under Grant Shen Fa Gai (2013) 1673.

The authors are with the Department of Electronic Engineering, The Chinese University of Hong Kong, Hong Kong (e-mail: zlli@ee.cuhk.edu.hk; klwu@ee.cuhk.edu.hk).

Color versions of one or more of the figures in this paper are available online at http://ieeexplore.ieee.org.

Digital Object Identifier 10.1109/TMTT.2017.2686863

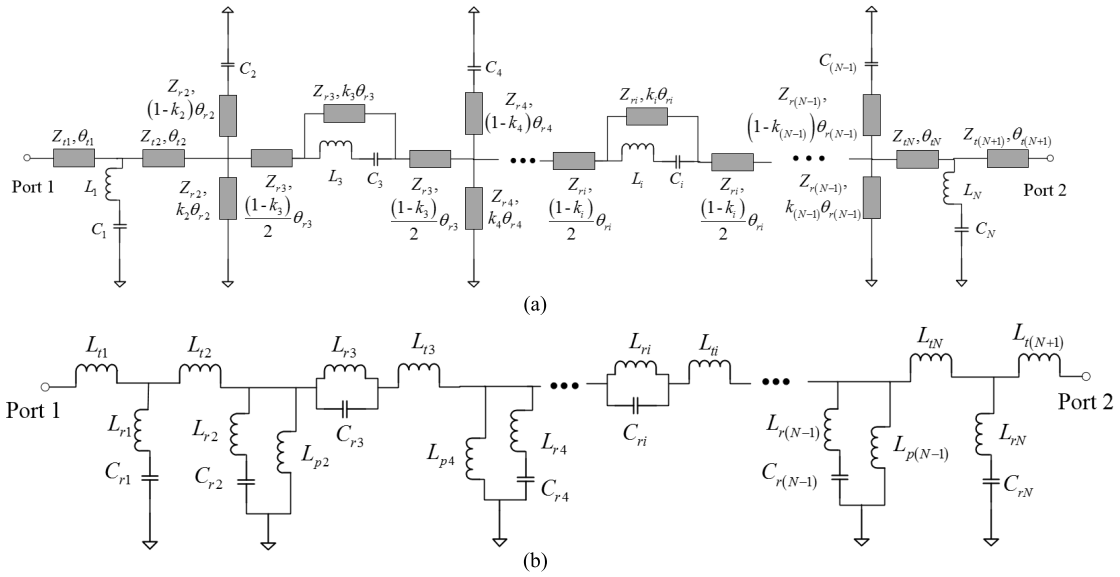

Fig. 1. Proposed Nth-order wideband filter with composite series and shunt resonators. (a) MLD circuit schematic and (b) its lumped element circuit representation.

high rejection level over a very wide upper stopband. With the circuit approximations introduced in [15] and two new approximations of shunt resonators for producing TZs in the far upper stopband and series resonators for TZs in the lower band, the mixed lumped/distributed (MLD) element circuit of the proposed filter can be directly synthesized and designed. The design process incorporates two steps: first, the lumped element surrogate circuit shown in Fig. 1(b) is exactly synthesized from specifications; then, the lumped element circuit is converted into the MLD element circuit on the basis of the circuit approximations in a wide frequency range for each basic circuit block.

This paper is organized as follows. The relative position between the TZ and transmission pole frequency for both composite series and shunt resonators is first demonstrated in Section II. In Section III, the synthesis theory of the lumped element circuit that is composed of both composite series and shunt resonators is discussed, from the filtering function to circuit model extraction. In Section IV, the approximations of shunt resonators for producing TZs in the far upper stopband and series resonators are introduced and verified. In Section V, the conversion process is elaborated from the synthesized lumped element circuit to a physically realizable MLD element circuit. Section VI discusses the design flexibility in a lumped element circuit topology, specifically, the benefits of removing the shunt inductors from the composite shunt resonators at the I/O ports. In Section VII, the method to suppress spurious resonances using TZs is thoroughly discussed through an example. Section VIII presents two practical design examples, demonstrating the synthesis and design theory and the attractive features of the proposed filter.

II. Composite Series and Shunt Resonators

To introduce TZs below the passband, composite series resonators are used here. For a composite series resonator as shown in Fig. 2(a), the TZ is produced when the *LC* tank

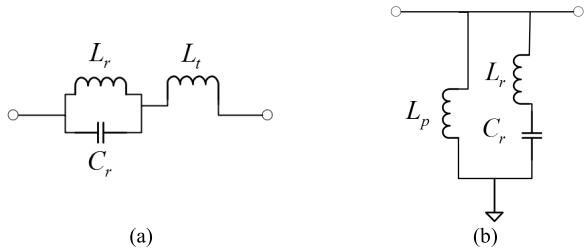

Fig. 2. Lumped element circuit model of (a) composite series resonator and (b) composite shunt resonator.

resonates. The TZ frequency f_z can be expressed as

$$f_z = \frac{1}{2\pi\sqrt{L_r C_r}}. \tag{1}$$

When the whole composite series resonator resonates, a short circuit is introduced between the two ends, contributing to a transmission pole. The pole frequency f_p can be found as

$$f_p = \frac{1}{2\pi\sqrt{L_r C_r}}\sqrt{1+\frac{L_r}{L_t}}. \tag{2}$$

By comparing (1) with (2), it can conclude that $f_p > f_z$, i.e., the TZ is located below the passband. Similarly, the composite shunt resonator as shown in Fig. 2(b) produces a transmission pole when the whole resonator resonates and a TZ when the *LC* series circuit resonates. The TZ frequency can be written in the same form as (1), and the pole frequency in the following form:

$$f_p = \frac{1}{2\pi\sqrt{(L_p+L_r)C_r}} \tag{3}$$

It is obvious that $f_p < f_z$ holds for the composite shunt resonator.

It is worth mentioning that the joint use of the composite series resonator and the composite shunt resonator in the filter configuration in Fig. 1(b) provides a new design option for wideband filters and has never been studied.

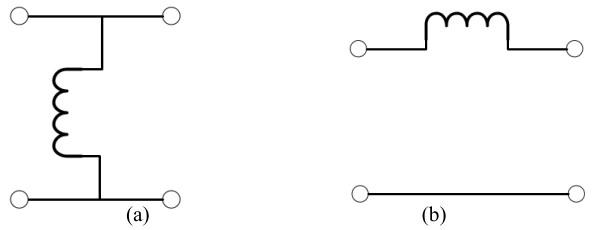

Fig. 3. Circuit configurations equivalent to the original lumped element circuit (a) dc and (b) infinity.

III. Synthesis of Lumped Element Circuit

For the lumped element circuit in Fig. 1(b), the reflection and transmission coefficients of the filter can be expressed as

$$S_{11} = \frac{F}{E} \quad S_{21} = \frac{P}{\varepsilon E} \tag{4}$$

where E, F, and P are real polynomials with the complex frequency variable $s = j\omega$, and ε is the ripple factor. The square magnitude of transmission coefficient can also be expressed as

$$|S_{21}|^2 = \frac{1}{1 + (\varepsilon F_N)^2} \tag{5}$$

where F_N is the filtering function and is related to F and P by

$$F_N = \frac{F}{P}. \tag{6}$$

To determine attributes of F_N, one can check the number of TZs located at finite nonzero frequencies, dc and infinity. The finite TZs are produced by either parallel connected *LC* series circuits or serially connected *LC* tanks, and they are all on the imaginary axis of the complex *s-plane*. The total number of finite TZs is N. The number of TZs at dc is the number of remaining elements after replacing all the inductors except shunt ones with short circuits and all the capacitors except series ones on the mainline with open circuits [23]. Similarly, the number of TZs at infinity is the number of remaining elements after replacing all the inductors except series ones on the main line with open circuits and all the capacitors except shunt ones with short circuits. As shown in Fig. 3, the circuit configurations that are equivalent to the original circuit in Fig. 1(b) at dc and infinity have an inductor alone. Therefore, there is one TZ at dc and one TZ at infinity. Since the finite TZs s_{zi} and that at dc are the roots of P, the factorized form of Pcan be expressed as

$$P = p_{2N+1} s \prod_{i=1}^{N} \left(s^2 - s_{zi}^2\right) \tag{7}$$

where $s_{zi} = jz_i$. As there is one TZ at infinity, the degree of F should be one order higher than that of P. Having understood the basic attributes of P and F, the rational expression of filtering function for the lumped element circuit in Fig. 1(b) can be constructed as

$$F_N = \frac{s^{2N+2} + f_{2N+1}s^{2N+1} + \cdots + f_1 s^1 + f_0}{p_{2N+1}s^{2N+1} + p_{2N-1}s^{2N-1} + \cdots + p_3 s^3 + p_1 s^1} \tag{8}$$

where coefficients f_0 through f_{2N+1} and p_1 through p_{2N+1} are real. Assuming that the roots of F are either on the imaginary axis of the s-plane or symmetrically located about the imaginary axis. Then, F must be an even polynomial and (8) can be simplified to

$$F_N = \frac{s^{2N+2} + f_{2N}s^{2N} + \cdots + f_2 s^2 + f_0}{p_{2N+1}s^{2N+1} + p_{2N-1}s^{2N-1} + \cdots + p_3 s^3 + p_1 s^1}. \tag{9}$$

It can be verified that the lumped element circuit in Fig. 1(b) possesses the property of

$$\frac{S_{11}|_{s=j0}}{S_{11}|_{s=j\infty}} = -1 \tag{10}$$

from which the existence of nonimaginary roots of F can be justified.

Equation (9) shares the same form of the filtering function with that proposed in [24] and used in [15] recently. Therefore, the same filtering function construction procedure can be used for the proposed lumped element circuit in Fig. 1(b), as is briefly given as follows:

$$F_N(\omega) = \cosh\left(\cosh^{-1}(F_1(\omega)) + \sum_{i=2}^{N} \cosh^{-1}(f_i(\omega))\right) \tag{11}$$

where

$$F_1(\omega) = \varepsilon_0 F_{1t}(\omega) = \varepsilon_0 (T_{0t}(\omega) f_{1t}(\omega) + G_t(\omega)) \tag{12}$$

$$T_0(\omega) = \frac{\omega^2 + \omega_1\omega_2}{(\omega_1 + \omega_2)|\omega|} \tag{13}$$

$$f_i(\omega) = \frac{T_1(\omega) - 1/T_1(z_i)}{1 - T_1(\omega)/T_1(z_i)} \tag{14}$$

$$T_1(\omega) = \frac{1}{\omega_2^2 - \omega_1^2}\left(2\omega^2 - \left(\omega_1^2 + \omega_2^2\right)\right) \tag{15}$$

$$G(\omega) = \frac{2\sqrt{\left(\omega_1^2 - z_1^2\right)\left(\omega_2^2 - z_1^2\right)}\left(\omega^2 - \omega_1^2\right)\left(\omega^2 - \omega_2^2\right)}{(\omega_1 + \omega_2)\left(\omega_2^2 - \omega_1^2\right)|\omega|\left(\omega^2 - z_1^2\right)} \tag{16}$$

$$\begin{cases} T_{0t}(\omega) = T_0(\omega)|\omega_1 = \omega_{1t}, \quad \omega_2 = \omega_{2t} \\ f_{1t}(\omega) = f_1(\omega)|\omega_1 = \omega_{1t}, \quad \omega_2 = \omega_{2t} \\ G_t(\omega) = G(\omega)|\omega_1 = \omega_{1t}, \quad \omega_2 = \omega_{2t} \end{cases} \tag{17}$$

where ω_1 and ω_2 are the lower and upper angular band edges, respectively. The prescribed TZs are denoted as z_i, and the rejection factor ε_0 is used to adjust the out-of-band rejection for the given passband and TZs z_i. With chosen ε_0, the intermediate frequencies ω_{1t} and ω_{2t} can be calculated by the criteria [24]

$$F_1(\omega_1) = \varepsilon_0 F_{1t}(\omega_1) = -1 \quad F_1(\omega_2) = \varepsilon_0 F_{1t}(\omega_2) = 1. \tag{18}$$

It is worth mentioning that ε_0 is always associated with z_1, and thus, z_1 should be designated for a given set of TZs. In fact, the filtering function is different even for the same ε_0 if the associated z_1 is different. To make the circuit shown in Fig. 1(b) realizable and its approximation accurate, a small value of ε_0 is chosen in design examples. From the filtering function, the polynomials E, F, and P are first obtained, and then used to calculate the overall *ABCD* matrix of the filter. Following the circuit synthesis approach described in [15],

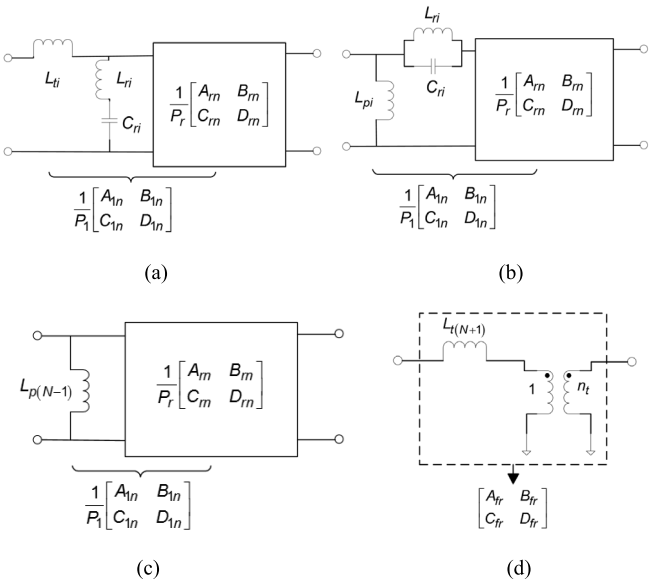

Fig. 4. Four basic circuit extraction operations. (a) Extraction of a series inductor and parallel connected LC series circuit. (b) Extraction of a shunt inductor and a serially connected LC tank. (c) Extraction of a shunt inductor. (d) Extraction of a series inductor and an ideal transformer.

circuit elements can be sequentially extracted from the *ABCD* matrix. Note that the arrangement of TZs is not unique but needs to be determined beforehand.

Fig. 4 illustrates four basic circuit extraction operations: 1) extracting a series inductor and a parallel connected LC series circuit; 2) extracting a shunt inductor and a serially connected LC tank; 3) extracting a shunt inductor $L_{p(N-1)}$; and 4) extracting the remainder circuit consisting of a series inductor $L_{t(N+1)}$ and an ideal transformer with ratio 1: n_t. In Fig. 4(a) and (b), the denominator polynomials P_1 and P_r are related by

$$P_1 = \left(s^2 - s_{zi}^2\right) P_r \tag{19}$$

where s_{zi} is the TZ assigned to the combination circuit of series L_{ri} and C_{ri}. In Fig. 4(c), the following relation can be obtained:

$$P_1 = s P_r. \tag{20}$$

For the circuit in Fig. 4(a), element values can be found by

$$L_{ti} = \frac{B_{1n}(s_{zi})}{s_{zi} D_{1n}(s_{zi})} \tag{21}$$

$$L_{ri} = \frac{s_{zi} B_{rn}(s_{zi})}{D_{1n}(s_{zi})} \quad C_{ri} = -1/(s_{zi}^2 L_{ri}) \tag{22}$$

where

$$B_{rn} = \frac{B_{1n} - s L_{ti} D_{1n}}{s^2 - s_{zi}^2}. \tag{23}$$

For the configuration in Fig. 4(b), element values can be found as

$$L_{pi} = \frac{B_{1n}(s_{zi})}{s_{zi} D_{1n}(s_{zi})} \tag{24}$$

$$L_{ri} = \frac{-B_{1n}(s_{zi})}{s_{zi}^3 D_{rn}(s_{zi})} \quad C_{ri} = -1/\left(s_{zi}^2 L_{ri}\right) \tag{25}$$

where

$$D_{rn} = \frac{1}{s^2 - s_{zi}^2}\left(D_{1n} - \frac{B_{1n}}{s L_{pi}}\right). \tag{26}$$

For the circuit in Fig. 4(c), the shunt inductance $L_{p(N-1)}$ contributes to the TZ at dc and can be extracted by

$$L_{p(N-1)} = -A_{rn}(0)/C_{1n}(0) \tag{27}$$

where

$$A_{rn} = A_{1n}/s. \tag{28}$$

The circuit elements in Fig. 4(d) can be extracted as

$$n_t = \frac{1}{A_{fr}} \quad L_{t(N+1)} = \frac{A_{fr} B_{fr}}{s}. \tag{29}$$

The entire extraction procedure for the circuit shown in Fig. 1(b) can be summarized as follows:

1) extracting L_{t1}, L_{r1}, and C_{r1} with (21)–(23);
2) extracting L_{t2}, L_{r2}, and C_{r2} with (21)–(23);
3) extracting L_{p2}, L_{r3}, and C_{r3} with (24)–(26);
4) extracting L_{t3}, L_{r4}, and C_{r4} with (21)–(23);
5) repeating the extraction of Fig. 4(a) and (b) alternatively until the parallel connected LC series circuit before extracting $L_{p(N-1)}$;
6) extracting $L_{p(N-1)}$ with (27) and (28);
7) extracting L_{tN}, L_{rN}, and C_{rN} with (21)–(23);
8) finally, the extraction procedure ends up at extracting $L_{t(N+1)}$ and n_t using (29).

Note that, even though the ideal transformer is not present in Fig. 1(b), it will generally be extracted with a nonunit transforming ratio. The transforming ratio n_t represents the degree of asymmetry of the filter circuit realization and is equal to unit if the filter circuit is symmetrical. As will be shown in design examples, n_t is close to unit due to the asymmetry.

IV. Approximation of Basic Circuit Elements

In order to convert the synthesized lumped element circuit into an MLD element circuit, an approximation of each basic circuit element and resonator in Fig. 1(b) must be introduced in a broadband sense. Since the approximations of coupling inductors L_{t1}, L_{t2}, L_{tN}, $L_{t(N+1)}$, and shunt resonators for producing close-to-band TZs are readily available in [15], only two new approximations need to be introduced here.

A. Approximation of Composite Shunt Resonator for Faraway TZ

As shown in Fig. 5, the composite shunt resonator consists of a parallel connected series LC and a shunt capacitor. Usually, the series LC circuit has a small inductance but a large capacitance as the produced TZ is in the far upper stopband, and the shunt capacitor that is originated from the coupling inductors is with negative shunt capacitance. The negative shunt capacitor will be absorbed by the series LC in the approximate circuit. The approximate circuit element

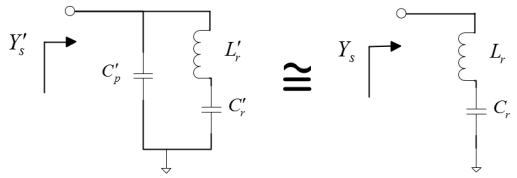

Fig. 5. Approximation of composite shunt resonator for producing faraway TZ.

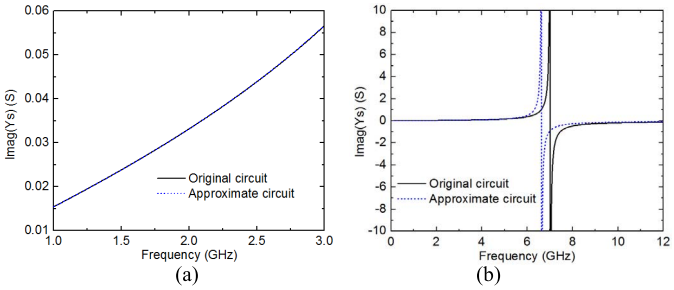

Fig. 6. Comparison between imaginary part of input admittances of composite shunt resonator and its approximate circuit in (a) passband and (b) broad frequency range.

values can be obtained by equating the input admittances of the two circuits in Fig. 5 at the band edges frequencies ω_1 and ω_2

$$j\omega C'_p - \frac{j\omega C'_r}{1-\omega^2 L'_r C'_r} = -j\frac{\omega C_r}{1-\omega^2 L_r C_r}, \quad \omega = \omega_1, \omega_2. \quad (30)$$

For example, when $L'_r = 0.19$ nH, $C'_r = 2.71$ pF, and $C'_p = -0.31$ pF, choosing $f_1 = 1.5$ GHz and $f_2 = 2.5$ GHz, the calculated results are $L_r = 0.24$ nH and $C_r = 2.40$ pF. The input admittances versus frequency are compared between the original circuit and its approximate circuit, as shown in Fig. 6. It can be seen that although the TZ shifts a little downward by the approximation, the admittances of the two models agree very well in the passband. The approximate circuit can be realized by a radial stub in a distributed circuit.

B. Approximation of Composite Series Resonator

As illustrated in Fig. 7(a), the composite series resonator consisting of an LC tank in series with an inductor can be approximated by a composite circuit that consists of a high-impedance transmission line (HITL) parallel connected with a capacitor C in series with an inductor L, and two shunt capacitors to the ground on both sides. The capacitor C can be realized by a surface mounted device chip capacitor, and inductor L represents a combination of parasitic inductor of the chip capacitor and the two short lines connecting the chip capacitor to the HITL. The number k represents the ratio of the electrical length of a partial HITL that is in parallel with the series LC circuit to the total electrical length of the HITL. The approximation is carried out at center frequency f_0 of filter as well as the TZ frequency, at which the following equation holds:

$$C = \frac{1}{\omega_z^2 L + \omega_z Z_r \sin(\frac{\omega_z}{\omega_0} k\theta_r)} \quad \omega_z = \frac{1}{\sqrt{L_r C_r}}. \quad (31)$$

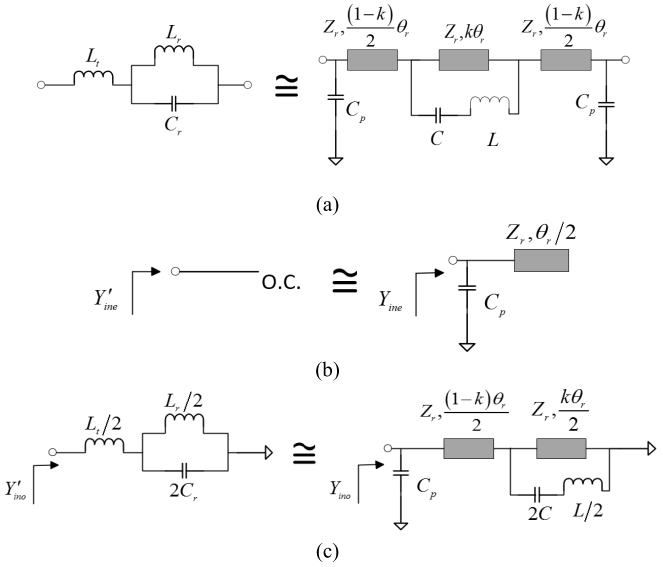

Fig. 7. (a) Composite series resonator and its MLD element approximation. (b) Even-mode bisected circuit. (c) Odd-mode bisected circuit.

The even-/odd-mode bisected circuits of a composite series resonator and their approximate circuits are shown in Fig. 7(b) and (c), respectively. The following equations can be obtained by equating their input admittances for even-/odd-mode case, respectively:

$$\omega_0 C_p = -Y_r \tan(\theta_r/2) \quad (32)$$

$$\frac{1-\omega_0^2 L_r C_r}{\omega_0^3 L_r C_r \frac{L_t}{2} - \omega_0 \frac{L_t}{2} - \omega_0 \frac{L_r}{2}} = \omega_0 C_p + Y_r \frac{\frac{2\omega_0 C}{Y_r\left(1-\omega_0^2 LC\right)} - \cot\left(\frac{k}{2}\theta_r\right) + \tan\left(\frac{1-k}{2}\theta_r\right)}{1-\left(\frac{2\omega_0 C}{Y_r\left(1-\omega_0^2 LC\right)} - \cot\left(\frac{k}{2}\theta_r\right)\right)\tan\left(\frac{1-k}{2}\theta_r\right)}. \quad (33)$$

Substituting (31) and (32) into (33), and designating Z_r, θ_r, and L, the ratio k can be found by solving (33). Then, C and C_p can be calculated using (31) and (32), respectively. For example, for $L_t = 1.756$ nH, $L_r = 2.871$ nH, $C_r = 6.127$ pF, and $f_0 = 2$ GHz, choosing Z_r as 100 Ω, with fixed $\theta_r = 35°$ at f_0, k and C can be plotted against L in Fig. 8(a). Alternatively, by fixing $L = 1.1$ nH, different k and C values can be obtained for different choices of θ_r, as shown in Fig. 8(b). It can be seen that there exists a wide range of capacitance values to choose from by changing L or θ_r. Therefore, one can always choose a capacitance value available for a chip capacitor. Fixing $L = 1.1$ nH and choosing different θ_r values, the responses of composite series resonator and its approximate circuits are compared in Fig. 9. It can be observed that $\theta_r = 35°$ is optimal for the minimal response deviation. Generally, to minimize the approximation error, a high Z_r and the optimal θ_r should be chosen, leaving L as the only design freedom. To make sure C is available by a chip capacitor, L should be appropriately designated.

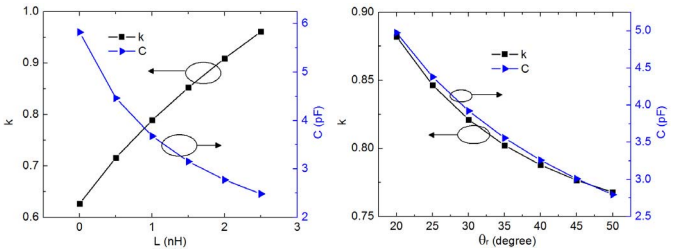

Fig. 8. Calculated k and C by (a) varying L but fixing $\theta_r = 35°$ and (b) varying θ_r but fixing $L = 1.1$ nH.

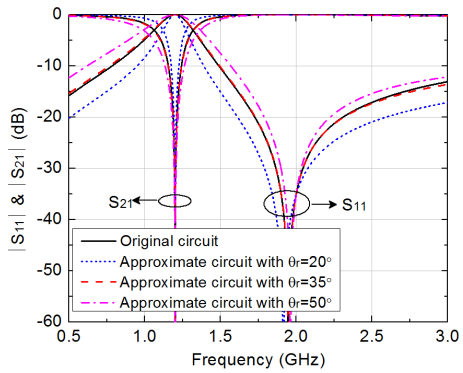

Fig. 9. Response comparison between composite series resonator and its approximate circuits with $\theta_r = 20°$, 35°, and 50°.

Note that, the shunt capacitor C_p is negatively valued and will be absorbed into the adjacent composite shunt resonators.

V. Conversion of Lumped Circuit to MLD Circuit

With the new approximations and those available in [15], the lumped element circuit in Fig. 1(b) can be systematically converted into the MLD element circuit in Fig. 1(a). As illustrated in Fig. 10, the conversion process can be summarized as follows.

1) The I/O coupling inductors L_{t1} and $L_{t(N+1)}$ are approximated by a piece of short transmission line cascaded to an ideal transformer and a shunt capacitor. The characteristic impedances Z_{t1} and $Z_{t(N+1)}$are chosen, such that the concerned transformers at the two ports share the same transforming ratio n_1 [15].
2) Then, the two identical symmetrically positioned transformers at the I/O ports could be shifted inward until they are next to each other. The two transformers can cancel out and all the lumped elements that are passed through by one of the transformers are scaled by a factor of n_1^2.
3) The interresonator coupling inductors L_{t2}, L_{tN}, and composite series resonators are then replaced by their approximate circuits.
4) Finally, all the composite shunt resonators are replaced by their approximate circuits.

Following the conversion process, a certain level of deviation between responses of the lumped and MLD element circuits will be inevitably introduced. The major deviation within the passband is due to the approximations of coupling inductors L_{t1}, L_{t2}, L_{tN}, $L_{t(N+1)}$, and composite series resonators. It can be found that the larger the inductances of coupling inductors and composite series resonators possess, the less accurate the two approximations are. To make sure these two approximations are accurate in a wide frequency range, a small value of ε_0 should be chosen so that those synthesized inductances in the lumped element circuit are small.

VI. Circuit Topologies

With the constructed filtering function according to the given specifications, the topology of the lumped element circuit in Fig. 1(b) is not unique, particularly the first and the last composite shunt resonators. As shown in Fig. 11, a fifth-order filter centered at $f_0 = 2$ GHz with 50% fractional bandwidth (FBW) is taken as an illustrative example. In Fig. 11(a), shunt inductors L_{p1} and L_{p5} are presented in the first and the last composite shunt resonators, respectively. Consequently, approximate circuits for these two resonators are the same as those for the other composite shunt resonators for producing close-to-band TZs, as depicted in Fig. 11(b). To obtain the lumped element circuit in Fig. 11(a), the element extraction procedure will be slightly different from that discussed in Section III. In the extraction, it is enforced that $L_{p1} = L_{p5}$. It is assumed that the in-band return loss is 20 dB and five TZs are arranged at 7, 2.7, 1.2, 2.7, and 6 GHz, counting from ports 1 to 2 or left to right in the filter circuit. The rejection factor ε_0 is set to 2 with the associated TZ at 2.7 GHz. Impedances of connecting lines and series resonators are set to 100 Ω. As shown in Fig. 12(a), with different values of L_{p1}, element values of the lumped element circuit and its corresponding MLD element circuit are varied. The electrical lengths of shunt resonators are chosen to be 60° at f_0, whereas electrical length of the series resonator is optimally chosen. As L_{p1} increases, both L_{p2} and L_{r3} decreases. The decrease of L_{p2} leads to a smaller Z_{r2}. As can be observed in Fig. 12(b), Z_{r1} is linearly related to L_{p1} approximately. A similar linear relation also exists between L_{p2} and Z_{r2}. Moreover, smaller L_{r3} allows a shorter electrical length of a series resonator, thereby pushing the spurious resonances away from the passband. This effect can be further demonstrated in Fig. 13.

Having understood the advantages of having large L_{p1} and L_{p5}, it is suggested that these two inductors are completely removed from the first and the last composite shunt resonators. There are two major benefits of removing the two-shunt inductors from the composite shunt resonators next to the two ports: 1) resulting smaller shunt inductors in the rest of composite shunt resonators and 2) having shorter electrical lengths in composite series resonators thus pushing further away spurious resonances. The former is especially important for large bandwidth filters, as they generally require large shunt inductances.

VII. Spurious Resonance Suppression Using TZs

To suppress the spurious resonances and to extend the stopband with a high rejection level, the TZs in the far

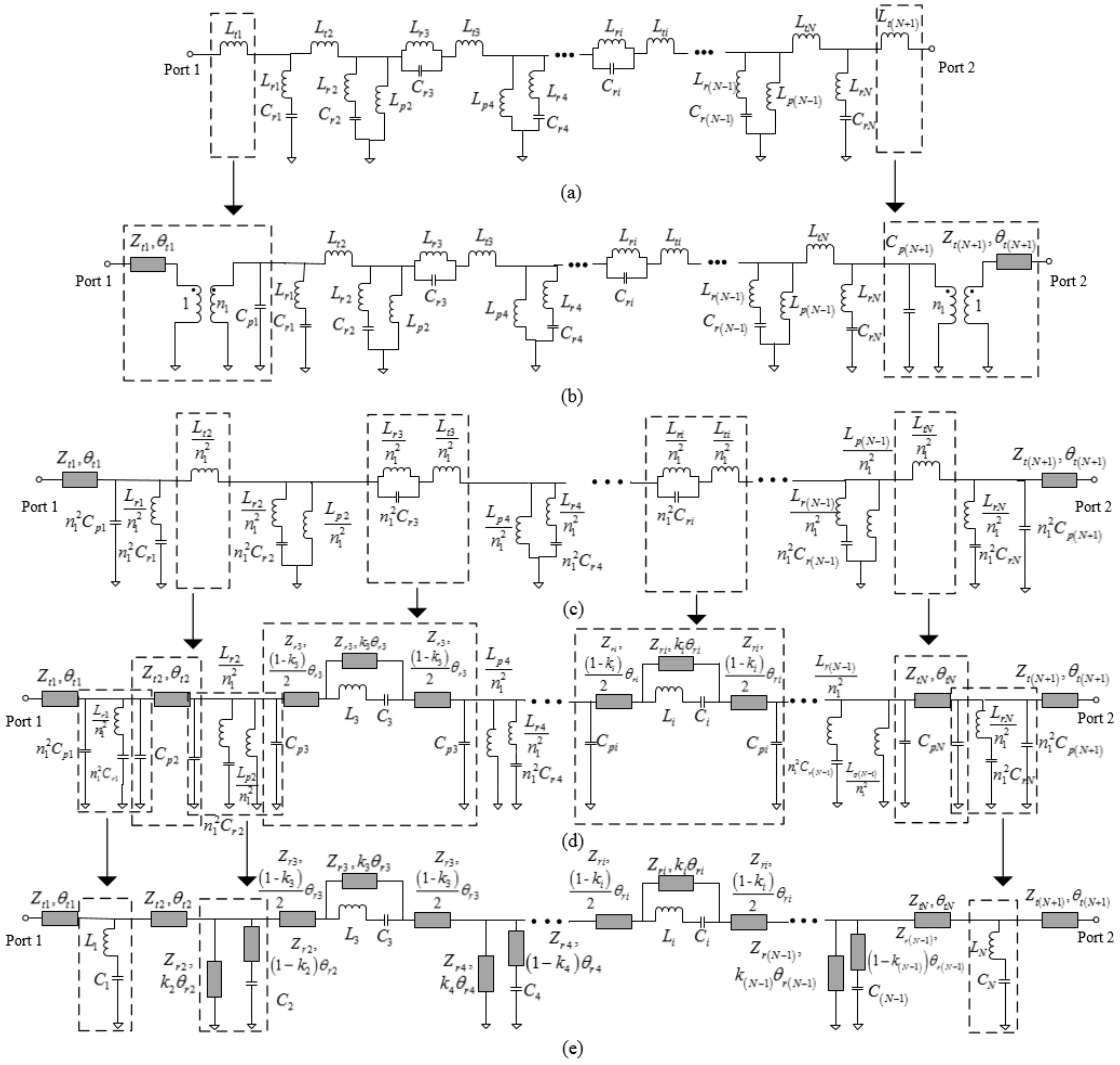

Fig. 10. Circuit in different stages of the conversion process. (a) Synthesized lumped element circuit. (b) Circuit after I/O coupling inductors approximated. (c) Circuit after lumped elements scaled. (d) Circuit after interresonator coupling inductors and composite series resonators approximated. (e) Final MLD element circuit after composite shunt resonators approximated.

stopband and electrical lengths of composite shunt resonators need to be appropriately designated. It is noteworthy that the electrical lengths of composite shunt resonators not only affect the spurious resonances but also high-order TZs. To illustrate how these factors affect the stopband performance, two different modifications to the example in Section VI are considered here. The first modification is to reassign the two far TZs at 4 GHz with other designations unchanged. The second modification is that the electrical lengths of composite shunt resonators, i.e., θ_{r2} and θ_{r4} are changed from 60° and 60° to 33° and 68°, respectively. Responses of the two modified MLD element circuits and that of the original one are shown in Fig. 14. In the range of 5–10 GHz, both original circuit and the first modified circuit have three spurious peaks, of which the first one and other two are caused by the composite series resonator and shunt resonators, respectively. In contrast, the second modified circuit has only two spurious peaks in that range, because its second composite shunt resonator has a much shorter electrical length θ_{r2}. With the first modification, the double TZs around 4 GHz are missaligned with the spurious resonances and fail to provide any suppression of spurious resonances. With far TZs assigned at 6 and 7 GHz, the original circuit achieves much better spurious suppression but still suffers from the relatively poor rejection around 8.4 GHz.

To further improve the rejection, the second modification is adopted by altering θ_{r2} and θ_{r4}. Here, θ_{r2} is first reduced by half so that only one spurious peak exists in the range of 8–10 GHz. Then, θ_{r2} and θ_{r4} are finely tuned so that the first high-order TZ produced by the fourth resonator cancels out the second spurious resonance. As shown in Fig. 14, the two narrow spurious peaks are still present after the second modification applied. Ideally, the spurious peaks can be perfectly suppressed with delicately assigned far TZs and designated electrical lengths of composite shunt resonators. However, the perfect suppression is unnecessary as those narrow spikes will be diluted due to finite Q values of resonators.

Considering spurious resonance suppression, a general synthesis and design procedure of the proposed wideband filter can be illustrated in Fig. 15. Since the spurious resonances

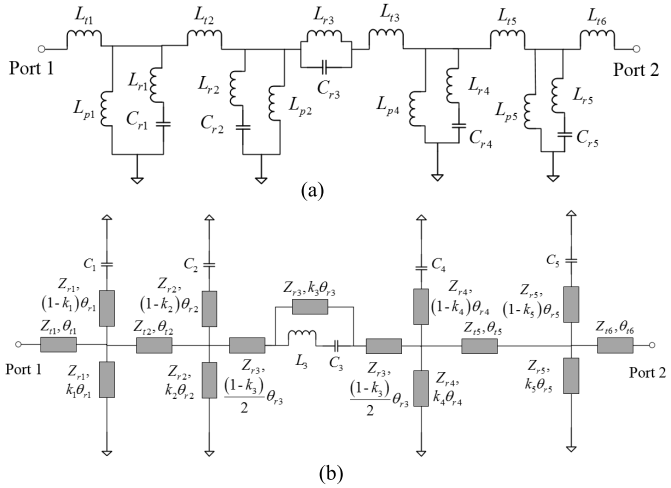

Fig. 11. Fifth-order filter with shunt inductors included in all the composite shunt resonators. (a) Lumped element circuit and (b) its MLD element approximate circuit.

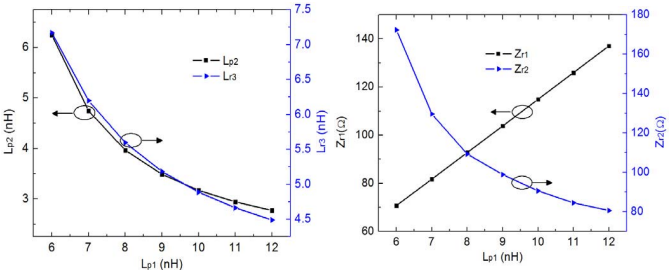

Fig. 12. Element values for different values of L_{p1}. (a) L_{p2} and L_{r3}. (b) Z_{r1} and Z_{r2}.

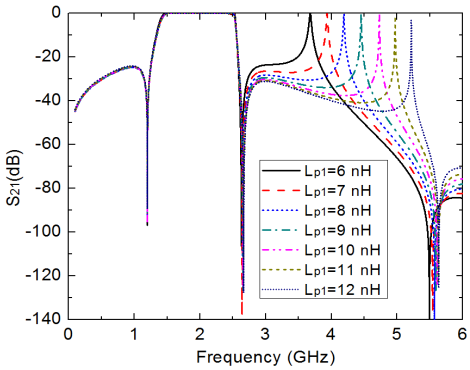

Fig. 13. Transmission responses of MLD element circuits for different values of L_{p1}.

are not known beforehand until the MLD element circuit of filter is obtained, the far TZs are aimlessly designated in the beginning. But after the first iteration of synthesis, their location can be almost determined. To achieve a satisfactory stopband performance, the procedure may take several iterations of fine tuning the far TZs and adjusting the electrical lengths of composite shunt resonators.

VIII. Design Examples

Two design examples are given here. The first one is the fifth-order wideband filter using the second modification as

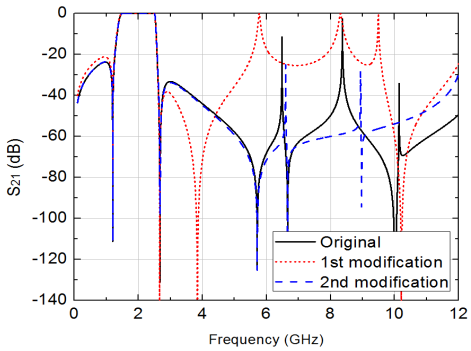

Fig. 14. Response comparison among the original designed circuit and two modified circuits.

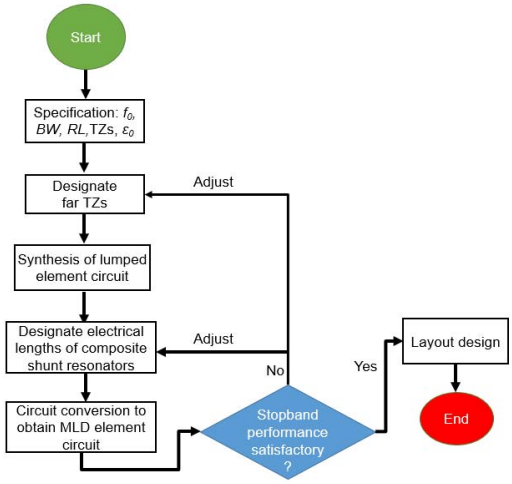

Fig. 15. Flowchart of synthesis and design procedure of the filter. *BW* and *RL* denote bandwidth and return loss, respectively.

TABLE I
CIRCUIT ELEMENT VALUES OF LUMPED ELEMENT CIRCUIT FOR EXAMPLE 1

L_{ti} (nH)	L_{pi} (nH)	L_{ri} (nH)	C_{ri} (pF)	n_t
L_{t1}=2.111 L_{t2}=2.072 L_{t3}=1.880 L_{t5}=2.011 L_{t6}=1.962	L_{p2}=1.592 L_{p4}=1.612	L_{r1}=0.204 L_{r2}=1.880 L_{r3}=3.073 L_{r4}=1.873 L_{r5}=0.283	C_{r1}=2.536 C_{r2}=1.849 C_{r3}=5.725 C_{r4}=1.855 C_{r5}=2.486	1.019

TABLE II
CIRCUIT ELEMENT VALUES OF MLD CIRCUIT FOR EXAMPLE 1

Z_{ti} (Ω)	θ_{ti} (°) @ f_0	Z_{ri} (Ω)	θ_{ri} (°) @ f_0	C_i (pF)	L_i (nH)	k_i
Z_{t1}=100 Z_{t2}=100 Z_{t5}=100 Z_{t6}=92.9	θ_{t1}=14.86 θ_{t2}=14.08 θ_{t5}=13.66 θ_{t6}=14.86	Z_{r2}=77.84 Z_{r3}=100 Z_{r4}=48.34	θ_{r2}=33 θ_{r3}=35 θ_{r4}=68	C_1=2.407 C_2=1.533 C_3=3.558 C_4=0.642 C_5=2.342	L_1=0.237 L_3=1.100 L_5=0.332	k_2=0.4033 k_3=0.8023 k_4=0.3122

discussed in Section VII. The element values of the lumped and MLD element circuit are listed in Tables I and II, respectively. The lumped element circuit is slightly asymmetrical and the extracted transforming ratio n_t is very close to unit, thus allowing the ideal transformer to be ignored. The responses of

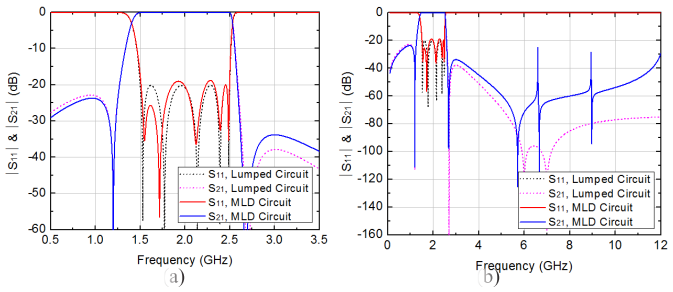

Fig. 16. Response comparison of the fifth-order filter in (a) passband and (b) broad frequency range.

the lumped and MLD element circuits are compared in Fig. 16. It shows that the responses agree well in the passband and have some frequency shift of far TZs in the upper stopband as expected. As discussed in Section VI, a TZ at 1.2 GHz and two TZs at 2.7 GHz are placed near to the passband to enhance the skirt selectivity. Two far TZs are assigned at 6 and 7 GHz, respectively, providing suppression of the first spurious resonance. By adjusting electrical lengths of composite shunt resonators that provide close-to-band TZs, the second spurious resonance is suppressed by the first high-order TZ from the fourth resonator. To implement the designed filter, the Rogers Duroid 5880 substrate with a relative permittivity of 2.2 and a thickness of 0.508 mm is used. The lumped capacitor C_3 in the series resonator is a 0402 3.6-pF chip capacitor.

With known characteristic impedances and electrical lengths of transmission lines, the widths and lengths of connecting lines and stubs can be determined. The tapping positions and dimensions of radial stubs are designed for each composite shunt resonator by matching the responses of their electromagnetic (EM) models and circuit models. The EM simulation is carried out in a commercial full-wave simulator, Ansys HFSS. In a similar way, the dimensions of a series resonator can be determined. The initial layout design of the filter can be obtained by simply cascading all designed resonators and connecting lines. Considering the parasitic couplings among adjacent resonators, a fine adjustment of dimensions is necessary to optimize the initial layout design. Note that the parasitic couplings among adjacent transmission lines are stronger if the used substrate is thicker. In such case, the dimensional adjustment could be relatively larger.

The final layout and the photograph of the fabricated filter are shown in Fig. 17. Table III shows the initial layout dimensions and optimized dimensional adjustments in parentheses. The small adjustments validate the direct synthesis and design theory. As can be seen from Fig. 18, the simulated and measured responses agree well with each other, except for some mismatch around the upper band edge due to losses. The matching can be further improved by fine tuning the dimensions. The measured insertion loss is 0.54 dB at the center frequency of 2 GHz. In the upper stopband, an overall rejection of 37 dB is achieved up to 11 GHz (5.5 f_0). The stopband performance has been well predicted by the MLD circuit simulation as shown in Fig. 16(b), from which the stopband can be extended to 11.8 GHz with 37-dB rejection. The skirt selectivity of the filter at upper band edge is higher

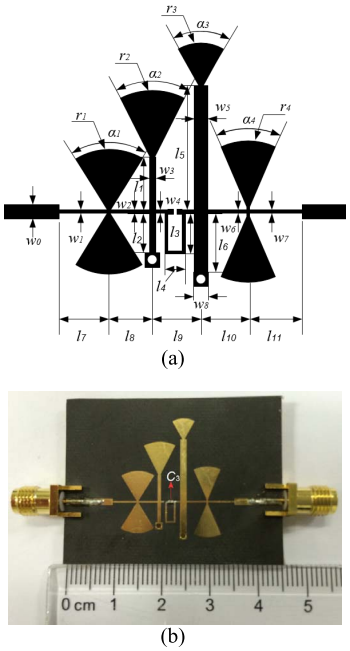

Fig. 17. (a) Layout. (b) Fabricated fifth-order filter.

TABLE III
FILTER INITIAL DIMENSIONS AND ADJUSTMENTS FOR EXAMPLE 1 (mm)

$w_0 = 1.40$ $w_1 = 0.33$ $w_2 = 0.33$ $w_3 = 0.69$ $w_4 = 0.33$ $w_5 = 1.40$ $w_6 = 0.33$ $w_7 = 0.39$ $w_8 = 1.50$	$l_1 = 5.68$ (-0.12) $l_2 = 3.99$ (+0.12) $l_3 = 4.23$ $l_4 = 2.12$ $l_5 = 13.44$ (-0.45) $l_6 = 5.69$ (+0.45)	$l_7 = 4.62$ (+0.55) $l_8 = 4.51$ $l_9 = 5.39$ (-0.38) $l_{10} = 4.45$ (+0.46) $l_{11} = 4.62$ (+0.95)	$r_1 = 6.6$ $r_2 = 7.4$ $r_3 = 4.9$ $r_4 = 7.2$	$\alpha_1 = 60.0°$ (+3.0°) $\alpha_2 = 52.7°$ (+0.6°) $\alpha_3 = 52.7°$ (+4.4°) $\alpha_4 = 45.0°$ (+0.9°)

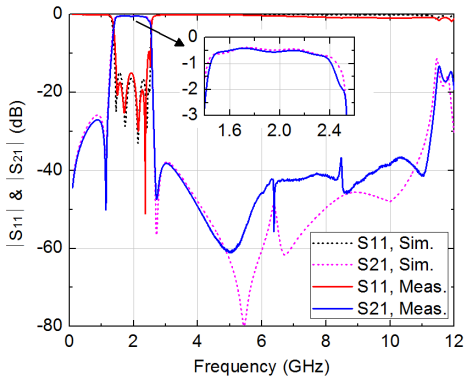

Fig. 18. Simulated versus measured responses of the fifth-order filter.

than that at lower band edge, because there are a double TZ at 2.7 GHz but a single TZ at 1.2 GHz. At the lower band edge, the skirt selectivity can be further enhanced by placing the lower band TZ closer to the passband.

The second design example is a ninth-order wideband filter with center frequency at 2 GHz, $FBW = 100\%$ and 20 dB in-band return loss. Following the synthesis and design procedure in Fig. 15, nine TZs are optimally arranged at 8.5, 6, 0.89, 3.3, 0.89, 3.3, 0.89, 7, and 8 GHz, for the resonators counting from

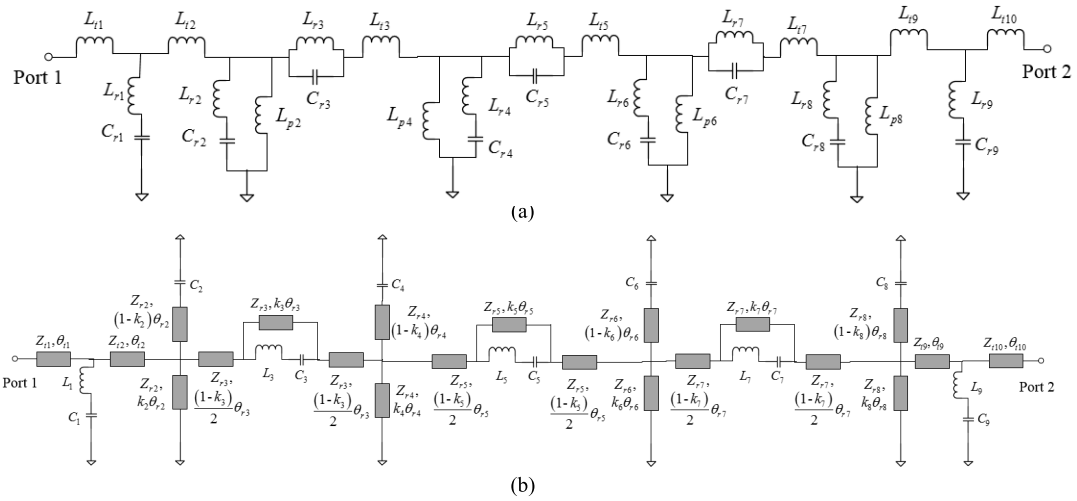

Fig. 19. Ninth-order wideband filter with all circuit parameters shown. (a) Lumped element circuit. (b) MLD element circuit.

TABLE IV
CIRCUIT ELEMENT VALUES OF LUMPED ELEMENT CIRCUIT FOR EXAMPLE 2

L_{ti} (nH)	L_{pi} (nH)	L_{ri} (nH)	C_{ri} (pF)	n_t
L_{t1}=0.395		L_{r1}=0.2182	C_{r1}=1.607	
L_{t2}=2.660		L_{r2}=0.2031	C_{r2}=3.464	
L_{t3}=2.109	L_{p2}=4.085	L_{r3}=3.805	C_{r3}=8.405	
L_{t5}=1.616	L_{p4}=3.882	L_{r4}=1.596	C_{r4}=1.457	
L_{t7}=2.155	L_{p6}=3.883	L_{r5}=4.755	C_{r5}=6.726	1.003
L_{t9}=2.703	L_{p8}=3.980	L_{r6}=1.599	C_{r6}=1.455	
L_{t10}=0.365		L_{r7}=3.816	C_{r7}=8.380	
		L_{r8}=0.1399	C_{r8}=3.694	
		L_{r9}=0.2501	C_{r9}=1.583	

TABLE V
CIRCUIT ELEMENT VALUES OF MLD ELEMENT CIRCUIT FOR EXAMPLE 2

Z_{ti} (Ω)	θ_{ti} (°) @ f_0	Z_{ri} (Ω)	θ_{ri} (°) @ f_0	C_i (pF)	L_i (nH)	k_i
				C_1=1.435		
		Z_{r2}=69.73	θ_{r2}=45	C_2=2.709		k_2=0.9320
Z_{t1}=100	θ_{t1}=2.844	Z_{r3}=100	θ_{r3}=43	C_3=5.538	L_1=0.270	k_3=0.7919
Z_{t2}=100	θ_{t2}=19.48	Z_{r4}=98.30	θ_{r4}=50	C_4=0.684	L_3=1.100	k_4=0.5436
Z_{t9}=100	θ_{t9}=19.80	Z_{r5}=100	θ_{r5}=47	C_5=4.690	L_5=1.100	k_5=0.8917
Z_{t10}=92.4	θ_{t10}=2.844	Z_{r6}=103.1	θ_{r6}=47	C_6=0.724	L_7=1.100	k_6=0.5522
		Z_{r7}=100	θ_{r7}=43	C_7=5.574	L_9=0.312	k_7=0.7854
		Z_{r8}=54.70	θ_{r8}=55	C_8=2.752		k_8=0.9485
				C_9=1.405		

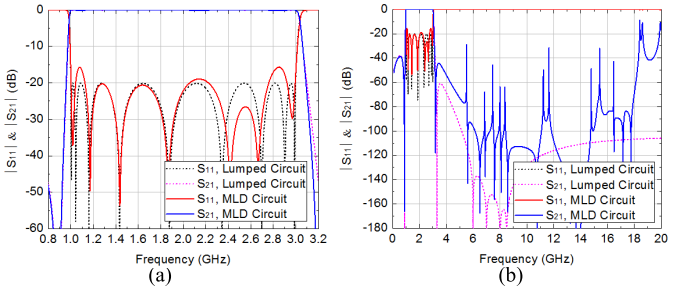

Fig. 20. Response comparison of the ninth-order filter in (a) passband and (b) broad frequency range.

left to right. The close-to-band TZs are placed at 0.89 and 3.3 GHz to achieve a steep skirt selectivity. The rejection factor ε_0 is set to 1.1 for the associated TZ at 3.3 GHz. Referring to Fig. 19, all circuit parameters are shown, and their values for the lumped and MLD element circuits are listed in Tables IV and V, respectively. The responses of lumped and MLD element circuits are compared in Fig. 20. As shown

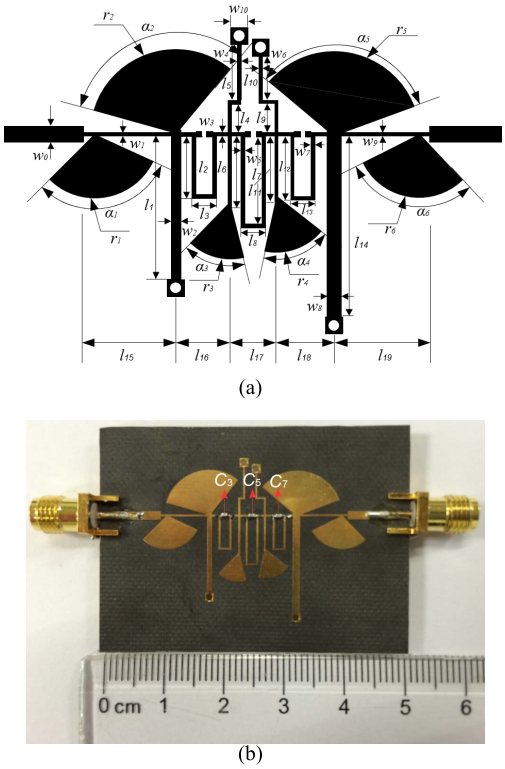

Fig. 21. (a) Filter layout. (b) Photograph of the ninth-order filter.

in Fig. 20(b), the stopband can be extended to 18 GHz (9 f_0) with approximate 40-dB rejection. The substrate used and the way to design the layout dimensions are the same as those used in the first design example. A 5.6-pF chip capacitor is used to realize C_3 and C_7, and a 4.7-pF chip capacitor is used to realize C_5. All chip capacitors are of 0402 sizes. Fig. 21 shows the layout and the photograph of the fabricated filter prototype. Table VI shows the initial layout dimensions and optimized dimensional adjustments. The simulated and measured responses are compared in Fig. 22. The measured insertion loss is about 0.57 dB at the center frequency of 2 GHz. In the upper stopband, a high rejection of 40 dB is achieved up to 14 GHz (7 f_0). The same rejection level is

TABLE VI

FILTER INITIAL DIMENSIONS AND ADJUSTMENTS FOR EXAMPLE 2 (mm)

w_0 = 1.40 w_1 = 0.33 w_2 = 0.77 w_3 = 0.33 w_4 = 0.35 w_5 = 0.33 w_6 = 0.31 w_7 = 0.33 w_8 = 1.20 w_9 = 0.33 w_{10} =1.50	l_1 = 12.54 l_2 = 5.55 (-0.11) l_3 = 2.12 l_4 = 2.49 l_5 = 4.86 l_6 = 6.28 l_7 = 6.51 (+1.11) l_8 = 2.12 l_9 = 2.53 l_{10} =3.86	l_{11} =5.74 l_{12} =5.55 l_{13} =2.12 l_{14}=15.89 (-0.05) l_{15} = 7.65 (+0.37) l_{16} = 6.16 (-1.48) l_{17} = 4.73 (-0.7) l_{18} = 6.48 (-1.50) l_{19} = 8.00 (+0.29)	r_1 = 5.49 r_2 = 7.40 r_3 = 4.90 r_4 = 4.90 r_5 = 7.40 r_6 = 5.50	α_1 = 109.8° α_2 = 118.6° (-5.2°) α_3 = 57.7° α_4 = 63.6° α_5 = 121.2° (-2.3°) α_6 = 106.6°

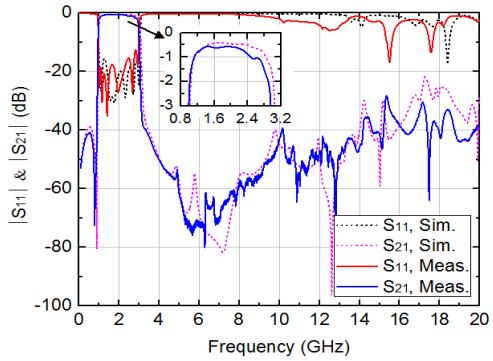

Fig. 22. Simulated versus measured responses of the ninth-order filter.

TABLE VII

COMPARISON WITH SOME PREVIOUS WIDEBAND FILTERS WITH SUPPRESSION OF SPURIOUS RESONANCES

Ref.	Order n	f_0 (GHz)	FBW (%)	Stopband limit	TZs on both sides?	Design method
[11]	---	0.64	110	6.7 f_0 (20 dB)	No	Opt./Tun.
[12]	4	5.6	80	2.6 f_0 (15 dB)	Yes	Opt./Tun.
[15]	8	2	50	4.5 f_0 (40 dB)	No	Syn.
[21]	5	6.2	97	3.2 f_0 (30 dB)	No	Opt./Tun.
[22]	6	1	42	5.6 f_0 (50 dB)	No	Opt./Tun.
This work	5	2	50	5.5 f_0 (37 dB)	Yes	Syn.
This work	9	2	100	7 f_0 (40 dB)	Yes	Syn.

Opt. — optimization; Tun. — tuning; Syn. — synthesis.

observed in the lower stopband. Note that the measured bandwidth of the upper stopband is narrower than that predicted in Fig. 20(b) due to the discrepancy between the MLD circuit model and the physical realization at the ultra-high frequency. This gap can be reduced by a fine tuning.

In practical applications, the filters may be required to be enclosed by a metal housing for EM shielding. To suppress the resonant modes of the housing, an absorbent material attached to the inside surfaces is usually necessary. It has been verified by experiments that after suppressing the housing resonances, the stopband performance of the two designed filters is almost the same as that of the filters being measured in an open space.

A comparison of the designed filters in this paper and other recently published wideband bandpass filters concerning suppression of spurious resonances is made in Table VII. As can be seen, the filters in this paper are obviously superior to other designs in exhibiting a higher rejection level over a wider stopband. Though the designed filter in [22] achieves a rejection level of 50 dB up to 5.6 f_0, there are no TZs on the lower side of the passband. Moreover, only [15] and this paper provide a direct synthesis and design procedure to determine circuit parameters systematically according to specifications.

IX. CONCLUSION

In this paper, a wideband bandpass filter composed of composite series and shunt resonators is proposed. Close-to-band TZs can be placed on both sides of the passband to enhance the skirt selectivity, whereas the far TZs can be used to suppress spurious resonances. With the proposed direct synthesis and design theory, the MLD element circuit model can be directly synthesized and the layout of filters can be directly designed. Through several iterations of reassigning far TZs and adjusting electrical lengths of shunt resonators, a wide stopband with a high rejection level can be achieved. Due to the presence of close-to-band TZs on both sides, a high and symmetrical skirt selectivity can be achieved. A very small dimensional adjustment in optimized layout validates the effectiveness of the synthesis and design theory. It is under investigation to realize the proposed filter configuration in a nonplanar form. It can be expected that the filter configuration and the design theory can find a wide range of applications in the industry.

REFERENCES

[1] W.-T. Wong, Y.-S. Lin, C.-H. Wang, and C. H. Chen, "Highly selective microstrip bandpass filters for ultra-wideband (UWB) applications," in *Proc. Asia–Pacific Microw. Conf.*, vol. 5. Dec. 2005, pp. 2850–2853.

[2] C.-L. Hsu, F.-C. Hsu, and J.-T. Kuo, "Microstrip bandpass filters for ultra-wideband (UWB) wireless communications," in *IEEE MTT-S Int. Microw. Symp. Dig.*, Jul. 2005, pp. 679–682.

[3] C. W. Tang and M. G. Chen, "A microstrip Ultra-wideband bandpass filter with cascaded broadband bandpass and bandstop filters," *IEEE Trans. Microw. Theory Techn.*, vol. 55, no. 11, pp. 2412–2418, Nov. 2007.

[4] L. Zhu, S. Sun, and W. Menzel, "Ultra-wideband (UWB) bandpass filters using multiple-mode resonator," *IEEE Microw. Wireless Compon. Lett.*, vol. 15, no. 11, pp. 796–798, Nov. 2005.

[5] L.-H. Hsieh and K. Chang, "Compact, low insertion-loss, sharp-rejection, and wide-band microstrip bandpass filters," *IEEE Trans. Microw. Theory Techn.*, vol. 51, no. 4, pp. 1241–1246, Apr. 2003.

[6] H. Ishida and K. Araki, "Design and analysis of UWB band pass filter with ring filter," in *IEEE MTT-S Int. Microw. Symp. Dig.*, vol. 3. Jun. 2004, pp. 1307–1310.

[7] S. Sun and L. Zhu, "Wideband microstrip ring resonator bandpass filters under multiple resonances," *IEEE Trans. Microw. Theory Techn.*, vol. 55, no. 10, pp. 2176–2182, Oct. 2007.

[8] H. Shaman and J. S. Hong, "Input and output cross-coupled wideband bandpass filter," *IEEE Trans. Microw. Theory Techn.*, vol. 55, no. 12, pp. 2562–2568, Dec. 2007.

[9] J.-Y. Li, C.-H. Chi, and C.-Y. Chang, "Synthesis and design of generalized Chebyshev wideband hybrid ring based bandpass filters with a controllable transmission zero pair," *IEEE Trans. Microw. Theory Techn.*, vol. 58, no. 12, pp. 3720–3731, Dec. 2010.

[10] W. J. Feng, W. Q. Che, Y. M. Chang, S. Y. Shi, and Q. Xue, "High selectivity fifth-order wideband bandpass filters with multiple transmission zeros based on transversal signal-interaction concepts," *IEEE Trans. Microw. Theory Techn.*, vol. 61, no. 1, pp. 89–97, Jan. 2013.

[11] R. Gómez-García, M.-Á. Sánchez-Soriano, M. Sánchez-Renedo, G. Torregrosa-Penalva, and E. Bronchalo, "Low-pass and bandpass filters with ultra-broad stopband bandwidth based on directional couplers," *IEEE Trans. Microw. Theory Techn.*, vol. 61, no. 12, pp. 4365–4375, Dec. 2013.

[12] C. Y. Hung, M. H. Weng, R. Y. Yang, and Y. K. Su, "Design of the compact parallel coupled wideband bandpass filter with very high selectivity and wide stopband," *IEEE Microw. Wireless Compon. Lett.*, vol. 17, no. 7, pp. 510–512, Jul. 2007.

[13] J. J. Sánchez-Martínez, E. Márquez-Segura, and S. Lucyszyn, "Synthesis and design of high-selectivity wideband quasi-elliptic bandpass filters using multiconductor transmission lines," *IEEE Trans. Microw. Theory Techn.*, vol. 63, no. 1, pp. 198–208, Jan. 2015.

[14] J. Bonache, I. Gil, J. García-García, and F. Martín, "Compact microstrip band-pass filters based on semi-lumped resonators," *IET Microw., Antennas Propag.*, vol. 1, no. 4, pp. 932–936, Aug. 2007.

[15] Z. Li and K.-L. Wu, "Direct synthesis and design of a general sequentially coupled wideband bandpass filter with N-transmission zeros," *IEEE Trans. Microw. Theory Techn.*, vol. 64, no. 5, pp. 1484–1495, May 2016.

[16] M. Makimoto and S. Yamashita, "Bandpass filters using parallel coupled stripline stepped impedance resonators," *IEEE Trans. Microw. Theory Techn.*, vol. MTT-28, no. 12, pp. 1413–1417, Dec. 1980.

[17] S.-C. Lin, P.-H. Deng, Y.-S. Lin, C.-H. Wang, and C. H. Chen, "Wide-stopband microstrip bandpass filters using dissimilar quarter-wavelength stepped-impedance resonators," *IEEE Trans. Microw. Theory Techn.*, vol. 54, no. 3, pp. 1011–1018, Mar. 2006.

[18] F. Huang, "Suppression of harmonics in microstrip filters with stagger tuning and voltage redistributions," *IEEE Trans. Microw. Theory Techn.*, vol. 62, no. 3, pp. 464–471, Mar. 2014.

[19] T. Lopetegi *et al.*, "New microstrip 'Wiggly-Line' filters with spurious passband suppression," *IEEE Trans. Microw. Theory Techn.*, vol. 49, no. 9, pp. 1593–1598, Sep. 2001.

[20] M.-A. Sanchez-Soriano, G. Torregosa-Penalva, and E. Bronchalo, "Multispurious suppression in parallel-coupled line filters by means of coupling control," *IET Microw., Antennas Propag.*, vol. 6, no. 11, pp. 1269–1276, Aug. 2012.

[21] H. N. Shaman and J.-S. Hong, "Compact wideband bandpass filter with high performance and harmonic suppression," in *Proc. 37th Eur. Microw. Conf.*, Munich, Germany, Oct. 2007, pp. 528–531.

[22] F. Huang, "Suppression of Harmonics in microstrip filters using a combination of techniques," *IEEE Trans. Microw. Theory Techn.*, vol. 63, no. 10, pp. 3453–3461, Oct. 2015.

[23] R. Saal and E. Ulbrich, "On the design of filters by synthesis," *IRE Trans. Circuit Theory*, vol. 5, no. 4, pp. 284–327, Dec. 1958.

[24] R. Zhang and L. Zhu, "Synthesis of dual-wideband bandpass filters with source–load coupling network," *IEEE Trans. Microw. Theory Techn.*, vol. 62, no. 3, pp. 441–449, Mar. 2014.

Zhiliang Li received the B.Eng. degree from the University of Electronic Science and Technology of China, Chengdu, China, in 2013. He is currently pursuing the Ph.D. degree at The Chinese University of Hong Kong, Hong Kong.

His current research interests include passive RF and microwave circuits and filters.

Ke-Li Wu (M'90–SM'96–F'11) received the B.S. and M.Eng. degrees from the Nanjing University of Science and Technology, Nanjing, China, in 1982 and 1985, respectively, and the Ph.D. degree from Laval University, Quebec City, QC, Canada, in 1989.

From 1989 to 1993, he was a Research Engineer and a Group Manager with the Communications Research Laboratory, McMaster University, Hamilton, ON, Canada. In 1993, he joined the Corporate Research and Development Division, COM DEV International, the largest Canadian space equipment manufacturer, where he was a Principal Member of Technical Staff. Since 1999, he has been with The Chinese University of Hong Kong, Hong Kong, where he is currently a Professor and the Director of the Radio frequency Radiation Research Laboratory. He has authored numerous publications in the areas of EM modeling and microwave passive components, microwave filter and antenna engineering. His current research interests include partial element equivalent circuit and physically derived micro-modeling circuits for high-speed circuits, RF and microwave passive circuits and systems, synthesis theory and robot automatic tuning of microwave filters, decoupling techniques for multiple antennas in both wireless terminals, and massive MIMO array antennas.

Prof. Wu is a member of the IEEE MTT-8 Subcommittee (Filters and Passive Components) and also serves as a TPC member of many prestigious international conferences, including the IEEE MTT-S International Microwave Symposium. He was an Associate Editor of the IEEE TRANSACTIONS ON MICROWAVE THEORY AND TECHNIQUES from 2006 to 2009. He was a recipient of the 1998 COM DEV Achievement Award for the development of exact EM design software of microwave filters and multiplexers and the Asia–Pacific Microwave Conference Prize in 2008 and 2012, respectively.